Mode Matching for Optical Antennas

Thorsten Feichtner,[1,2,3] Silke Christiansen,[1,2,4] and Bert Hecht[3,*]
[1]Helmholtz-Zentrum Berlin für Materialien und Energie GmbH, Institut Nanoarchitekturen für die Energieumwandlung, Hahn-Meitner-Platz 1, 14109 Berlin, Germany
[2]Max Planck Institute for the Science of Light, Staudtstrasse 2, 91058 Erlangen, Germany
[3]Nano-Optics & Biophotonics Group, Department of Experimental Physics 5, Röntgen Research Center for Complex Material Research (RCCM), Physics Institute, University of Würzburg, Am Hubland, 97074 Würzburg, Germany
[4]Freie Universität Berlin, Arnimallee 14, 14195 Berlin, Germany
(Received 18 November 2016; published 21 November 2017)

The emission rate of a point dipole can be strongly increased in the presence of a well-designed optical antenna. Yet, optical antenna design is largely based on radio-frequency rules, ignoring, e.g., Ohmic losses and non-negligible field penetration in metals at optical frequencies. Here, we combine reciprocity and Poynting's theorem to derive a set of optical-frequency antenna design rules for benchmarking and optimizing the performance of optical antennas driven by single quantum emitters. Based on these findings a novel plasmonic cavity antenna design is presented exhibiting a considerably improved performance compared to a reference two-wire antenna. Our work will be useful for the design of high-performance optical antennas and nanoresonators for diverse applications ranging from quantum optics to antenna-enhanced single-emitter spectroscopy and sensing.

DOI: 10.1103/PhysRevLett.119.217401

Introduction.—Focusing optical antennas (FOAs) make use of plasmonic resonances to convert propagating electromagnetic waves at visible frequencies to near fields localized in nanoscale volumes much smaller than the diffraction limit [1,2]. In such a hot spot the local density of states (LDOS) for pointlike quantum emitters (QEs) may be increased by a factor of 10^3 and possibly beyond [2–4], which can be applied in novel light-based technologies, e.g., quantum optics [5] and communication [6], sensing [7], as well as scanning near-field microscopy [8]. The design of FOAs, which typically consist of single or multiple particles of basic shapes [3,6,9–11], is largely inspired by rules derived from the radio frequency (rf) regime. The resulting antenna structures, however, can hardly be optimal for QE-FOA coupling, since there is no comparable task in rf technology. In addition, the radiation behavior of optical antennas differs from their rf counterparts due to Ohmic losses and fields penetrating the antenna material [12]. Yet, it has been shown that the Purcell factor [13,14] and likewise the antenna impedance [15] provide a measure for emitter-antenna coupling based on the antenna's Green's function [16].

Here, we combine Poynting's theorem [17] with reciprocity [18] to quantify QE-FOA coupling by means of a 3D overlap integral of the QE's electric field and the antenna mode current pattern (cf. mode matching [19,20]). Introducing a further mode-matching condition for FOA to far-field coupling allows us to identify two independent FOA mode current patterns, which both maximize antenna radiation. This enables us to understand the high performance of FOAs obtained from evolutionary optimization [21] as well as of other unusual FOA geometries, like the indented nanocone [22] or the double hole resonator [23]. Finally, based on our new design rules, an improved plasmonic cavity antenna geometry is devised and numerically investigated. The flexibility of the presented framework opens diverse applications ranging from improved emitter-cavity coupling in quantum optics to enhanced single-emitter sensing schemes. It also provides new insights for the understanding and optimization of complex-shaped metal nano-objects as they appear in surface-enhanced Raman scattering (SERS) substrates [24].

Theory.—We consider a point dipole with dipole moment $\mathbf{p}$ situated at $\mathbf{r}_p$, emitting photons at wave number k with unity quantum efficiency. The emitted power P of the dipole in an arbitrary environment depends on the self-interaction due to scattered fields $\mathbf{E}_{\mathrm{sc}}$. The enhancement of the QE emission rate γ/γ_0 as well as of the dipole emission power P/P_0 in an inhomogeneous environment can be calculated based on Poynting's theorem in Systeme International units [17]:

$$\frac{\gamma}{\gamma_0} = \frac{P}{P_0} = 1 + \frac{6\pi\varepsilon_0}{|\mathbf{p}|^2}\frac{1}{k^3}\mathrm{Im}\{\mathbf{E}_{\mathrm{sc}}(\mathbf{r}_p)\cdot\mathbf{p}^*\}. \quad (1)$$

Here, γ_0 and P_0 are the vacuum values of the QE emission rate and dipole emission power, respectively. The emission power enhancement depends on the backscattered field components at the dipole position parallel to the dipole moment. Equation (1) also takes into account the phase between the dipolar moment and scattered field $\Delta\phi = \phi_{\mathrm{sc}} - \phi_p$ [25],

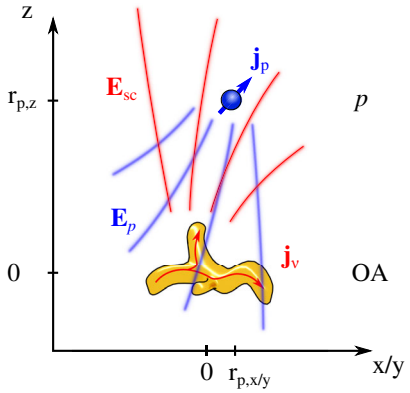

FIG. 1. General setup of a dipole p situated at $\mathbf{r}_p$ with an oscillating current $\mathbf{j}_p$ being the source of electromagnetic fields $\mathbf{E}_p$. In its environment a metallic nanoparticle is situated with a single excitable mode ν leading to scattered fields $\mathbf{E}_{p/\nu}$ originating from source current densities $\mathbf{j}_{p/\nu}$.

$$\mathrm{Im}\{\mathbf{E}_{\mathrm{sc}}(\mathbf{r}_p)\cdot\mathbf{p}^*\} = |\mathbf{E}_{\mathrm{sc}}(\mathbf{r}_p)|\cdot|\mathbf{p}|\cdot\mathrm{Im}\{e^{i\Delta\phi}\}. \quad (2)$$

We define the scattering environment to be a general FOA with its center of mass in the coordinate origin as sketched in Fig. 1. It exhibits a set of plasmonic eigenmodes at the emission wavelength of the QE, which is positioned at $\mathbf{r}_p$ near the FOA with $\mathbf{k}\cdot\mathbf{r}_p \ll 1$. Its current density then can be written as $j_p = -i\omega\mathbf{p}\delta(\mathbf{r}-\mathbf{r}_p)$. In the following we assume without loss of generality only a single relevant FOA mode ν to be the source of the scattered field $\mathbf{E}_{\mathrm{sc}}$ in Eqs. (1) and (2), which can be expressed as

$$\mathbf{E}_{\mathrm{sc}}(\mathbf{r}_p) = i\omega\mu_0\int_{V_\nu}\bar{\mathbf{G}}_0(\mathbf{r}_p,\mathbf{r}')\mathbf{j}_\nu(\mathbf{r}')d^3r', \quad (3)$$

where $\bar{\mathbf{G}}_0(\mathbf{r}_p,\mathbf{r}')$ is the Green's tensor and $\mathbf{j}_\nu$ is the antenna mode current density, being the source of the scattered field. The mode current density is derived from the quasinormal eigenmode electric field distribution $\mathbf{E}_\nu$ of the optical antenna, which incorporates also the far-field radiation [13,26–28] (see Sec. S1 of the Supplemental Material [29] for details about the determination of E_ν). The currents inside the antenna are then obtained via $\mathbf{j}_\nu = \sigma\cdot\mathbf{E}_\nu$, where σ is the frequency and material dependent conductivity.

We now restrict the setup to the quasistatic limit. Then, for a FOA consisting of a local, dispersive, and lossy material, which is described by the dielectric function $\varepsilon(\omega)$, the reciprocity theorem implies the symmetry $\bar{\mathbf{G}}(\mathbf{r}_p,\mathbf{r}') = \bar{\mathbf{G}}(\mathbf{r}',\mathbf{r}_p)$ of the Green's tensor [18,30]. Inserted into Eq. (3) the scattered fields now depend on the Green's function of the emitting dipole at $\mathbf{r}_p$ evaluated inside the volume of the FOA:

$$\mathbf{E}_{\mathrm{sc}}(\mathbf{r}_p) = i\omega\mu_0\int_{V_\nu}\bar{\mathbf{G}}_0(\mathbf{r}',\mathbf{r}_p)\mathbf{j}_\nu(\mathbf{r}')d^3r'. \quad (4)$$

In the quasistatic limit $\mathbf{k}\cdot\mathbf{d} \ll 1$ with $\mathbf{d} = (d_x, d_y, d_z)$ being the spacial extension vector of the optical antenna, containing the maximal extents in all three dimensions, and $\mathbf{k}$ being the incoming wave vector. This ensures that all current elements contribute with the same phase to the scattered field at the dipole position (see Sec. S3 [52] for a generalization beyond the quasistatic approximation). As we are working at the antenna resonance, we have $\Delta\phi = \pi/2$ and thus $\mathrm{Im}\{e^{i\Delta\phi}\} = 1$, which allows us to simplify Eq. (2) to $\mathrm{Im}\{\mathbf{E}_{\mathrm{sc}}(\mathbf{r}_p)\cdot\mathbf{p}^*\} = |\mathbf{E}_{\mathrm{sc}}(\mathbf{r}_p)|\cdot|\mathbf{p}|$. Introducing this together with Eq. (4) into Eq. (1) then yields

$$\frac{\gamma}{\gamma_0} = \frac{P}{P_0} = 1 + \frac{6\pi\varepsilon_0}{|\mathbf{p}|^2}\frac{1}{k^3} \times \omega\mu_0\int_{V_\nu}|\bar{\mathbf{G}}_0(\mathbf{r}',\mathbf{r}_p)\mathbf{p}\mathbf{j}_\nu(\mathbf{r}')|d^3r'(\mathbf{r}_p). \quad (5)$$

Using $\mathbf{E}_p(\mathbf{r}) = \omega^2\mu_0\bar{\mathbf{G}}(\mathbf{r},\mathbf{r}_p)\mathbf{p}$ we obtain the important result

$$\frac{P}{P_0} = 1 + \frac{6\pi c\varepsilon_0}{k^4}\int_{V_\nu}|\mathbf{E}_p(\mathbf{r}')\cdot\mathbf{j}_\nu(\mathbf{r}')|d^3r' \quad (6)$$

with c the speed of light in vacuum. This equation describes the fact that the total power extracted from a point dipole into the νth antenna mode (i.e., the Purcell factor) is described by the overlap integral of the mode's current density pattern with the point dipole fields inside the volume of the FOA, thereby defining a mode-matching condition. Equation (6) is a variation of the volume integral equation formalism for electromagnetic scattering [31] and it has been derived in this context before [32,33]. However, until now Eq. (6) has not been interpreted in the context of optical antennas to derive design rules as presented in the following section.

To test the validity of Eq. (6), the analytical case of a dipole in front of a sphere has been evaluated (see Sec. S2 of the Supplemental Material [29], including Refs. [34–39]) and a numerical test on split-ring antennas has been performed (see Sec. S3 of the Supplemental Material [29], including Ref. [40]). A phase-dependent formulation of Eq. (6) that is valid beyond the quasistatic approximation and, thus, can be extended also for multiple resonances is derived and discussed in Sec. S4 of the Supplemental Material [29]. We also point out that for radio-frequency antennas the integration in Eq. (6) can be restricted to the surface of a perfect-metal antenna.

Discussion.—Equation (6) is reminiscent of the mode matching formalisms used to determine the coupling efficiencies between waveguide modes [19,20]. Here, however, the three-dimensional volume of the FOA has to be considered. From Eq. (6) three intuitive rules can be deduced. (i) Align the dipole field and the antenna's mode current pattern everywhere inside the antenna volume. (ii) Maximize the mode current $\mathbf{j}_\nu = \sigma\cdot\mathbf{E}_\nu$ at each point inside the plasmonic antenna. The field amplitude $|E_\nu|$ of the

quasinormal eigenmode ν inside the antenna material is frequency dependent, showing a Lorentz peak at the position of the antenna resonance. Both the antenna geometry and the material's complex dielectric function define the position of the resonance peak and can be used to maximize E_ν at the emission frequency of the dipole. The conductivity σ is a frequency-dependent material property and, therefore, the antenna material should be chosen to show a large σ at the emission frequency of the dipole (compare Sec. III. 2 in Ref. [33]). (iii) Maximize the volume of the overlap integral. This suggests the use of as much metal as possible in the vicinity of the dipole. Rules (i) and (iii) suggest that the established two-particle geometries may not result in the best possible FOAs. Instead, a FOA should enclose the QE as much as possible, resembling a kind of plasmonic cavity antenna. Antennas that to some extend fulfill these design rules in two dimensions have already been realized and are known as double-hole resonators [23].

So far we have only considered the transfer of energy from the dipole to the antenna mode. However, a FOA has two tasks, which have to been fulfilled simultaneously by the antenna mode: in addition to providing a maximal LDOS at the emitters' position it also has to couple efficiently to propagating far fields [41]. Therefore, we introduce a second dipole in the far field oriented parallel to the first dipole representing a pointlike detector or—since reciprocity applies—a pointlike emitter. The mode-matching formalism according to Eq. (6) can then also be used to describe the coupling to this second dipole in the far field. As the antenna can be described quasistatically the electric fields of the second dipole in the FOA volume can be approximated as plane waves corresponding to a homogeneous field $\mathbf{E}_f$ parallel to the far-field dipole moment. To optimize far-field coupling the mode currents of the optical antenna should therefore be parallel to $\mathbf{E}_f$ in accordance with rule (i).

In order to find a mode current distribution that optimizes coupling to both the near-field and the far-field dipole, $\mathbf{E}_f$ can be superposed linearly on the near fields $\mathbf{E}_n$ originating from the dipole close to the antenna. For a QE oriented along the x axis the optimal mode current pattern to fulfill both mode-matching criteria is therefore a linear combination of the quasistatic dipolar contribution

$$\mathbf{E}_n = \frac{1}{4\pi\varepsilon_0}\frac{3\mathbf{n}(\mathbf{np}) - \mathbf{p}}{r^3} \tag{7}$$

with the homogeneous field $\mathbf{E}_f = a\hat{\mathbf{x}}$:

$$\mathbf{E}_\nu = \mathbf{E}_n + \mathbf{E}_f. \tag{8}$$

The scalar factor a can be positive or negative, leading to two fundamentally different optimal focusing antenna mode current patterns as illustrated in Fig. 2(a), which we denote as the "n-type" (left) and "p-type" (right) mode. Close to the antenna hot spot in which the QE is positioned the dipolar near field $\mathbf{E}_n$ dominates. Away from the QE, $\mathbf{E}_n$ falls off as $1/r^3$ and the homogeneous field starts to dominate. For the n-type mode (p-type mode) isolated points on the x axis (a continuous circle in the yz plane) with zero field strength appear (marked with white dashed circles).

Figure 2(b) shows a mode current pattern of a FOA that resulted from an evolutionary algorithm [21,42–45] with the optimization goal to maximize the near field in the center of the structure using a planar 30 nm thick patterned gold layer at $\lambda = 830$ nm illuminated by a horizontally polarized focused Gaussian beam. The current pattern is identified as a p-type mode (areas with vanishing fields marked with a white dashed line): the antenna center is surrounded by gold, realizing the 2D equivalent of a plasmonic cavity antenna. The currents switch direction on the y axis to match the needs for optimal far-field coupling. Since the antenna is sufficiently small and centered in a Gaussian focus, a plane wave excitation can be assumed. While a p-type mode current pattern can be obtained in this 2D arrangement it cannot be realized with benefits in 3D as discussed in Sec. S5 of the Supplemental Material [29] (including Refs. [46–48]).

Figure 2(c) introduces a 3D plasmonic cavity antenna supporting the n-type mode current pattern, which to our knowledge has not yet been realized in an optical antenna [49]. We choose a geometry with rotational symmetry based on a reference antenna [two-wire dipole antenna, 10 nm gap, 15 nm wire diameter, spherical end caps, overall length $l = 110$ nm, made from gold, see the small black inset in Fig. 2(d)]. The reference antenna has a resonance at $\lambda = 650$ nm [black graph, Fig. 2(d)]. To realize the plasmonic cavity antenna, interconnects were attached between the antenna arms to allow additional current paths, enclosing the QE with gold. The length of the plasmonic cavity antenna was tuned to also be resonant at $\lambda = 650$ nm resulting in a slightly reduced length of $l = 104$ nm, 5.5% shorter than the reference antenna. The plasmonic cavity antenna is a single particle with a mode current pattern flowing unidirectionally from end to end resembling a $\lambda/2$ resonance [see the inset of Fig. 2(c)]. The mode current pattern also exhibits areas of vanishing fields along the x axis, as expected for an n-type mode [left panel of Fig. 2(a)]. In contrast, the reference antenna exhibits a λ resonance [see Fig. A1(b) of the Supplemental Material [29]] similar to voltage-fed radio-frequency antennas (Table 3.1, p. 45 in Ref. [51]).

Figure 2(d) shows the near-field intensity enhancement spectra at the antenna center for both the plasmonic cavity antenna and reference antenna when illuminated by a Gaussian focus with a numerical aperture NA = 1. Since both antennas exhibit a dipolar emission pattern, Gaussian excitation can also be used—in the same way as plane wave excitation—to investigate relative changes in the antenna's far-field coupling. Both antenna resonances peak at $\lambda = 650$ nm with a near-field intensity enhancement of 2.79×10^3 (2.08×10^3) for the plasmonic cavity antenna (reference antenna) and a Q factor $= \lambda/\Delta\lambda$ of 22.0 (27.1).

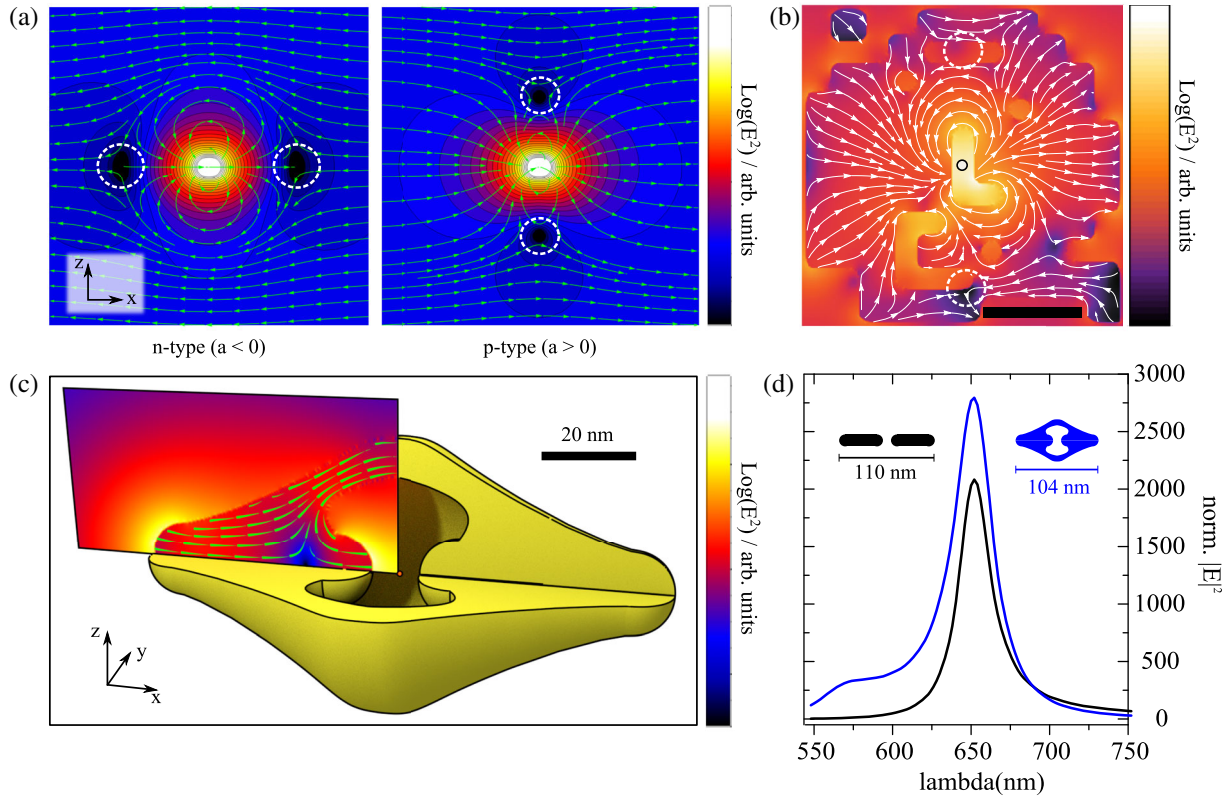

FIG. 2. Plasmonic antenna modes with double mode matching. (a) xy cross section of the linear combination of a quasistatic dipolar field and a constant field pointing in the x direction as described by Eq. (8) for $a < 0$ (left) and $a > 0$ (right). The white dashed circles mark the points of vanishing fields for better orientation in panel (b), showing the near field intensity enhancement (color scale) and the current direction (white arrows) of a planar antenna geometry optimized by an evolutionary algorithm for maximum fields in the center (marked by a small circle, scale bar: 100 nm) [21]. (c) Antenna design carrying a resonant mode resembling panel (a), left. The originally rotational symmetric geometry is shown with a 90° cutaway for improved visualization. Additionally, the near-field intensity (color) as well as the current direction (green arrows) are overlaid for a quarter cross section. The small orange dot marks the center, where a QE is to be placed. (d) Near-field intensity enhancement spectra at the orange point in panel (c) (blue) as well as at the center of a two-wire dipole reference antenna, with an identical end cap radius (black). The small insets show the xy plane cross section of both geometries.

The plasmonic cavity antenna spectrum shows a second shallow peak at 570 nm, due to a mode similar to that of the reference antenna with a current density in the x direction that does not change its direction. An analysis of the antenna cross sections under plane wave illumination was performed to characterize the far-field coupling and identify the additional loss channels of the plasmonic cavity antenna that lead to the 19% decreased Q factor. The plasmonic cavity antenna exhibits an absorption cross section of 4.17×10^4 nm^2 and a scattering cross section of 1.77×10^4 nm^2, yielding a scattering efficiency of $\eta = 0.298$. The reference antenna exhibits an absorption cross section of 2.34×10^4 nm^2 and a scattering cross section of 0.362×10^4 nm^2 and, thus, a 55% lower scattering efficiency of $\eta = 0.134$. Thus, the lowered Q factor for the plasmonic cavity antenna is due to increased radiation losses. According to Ref. [52], particles small compared to the impinging wavelength couple best to the far field, when the scattering and absorption cross sections are equal. Also, the plasmonic cavity antenna mode currents from end to end resemble those that of a $\lambda/2$ antenna, which in rf technology is known to radiate most efficiently [51].

Although realizing an n-type mode current pattern, the plasmonic cavity antenna design in Fig. 2(c) likely does not represent the ultimate limit that can be achieved in terms of near-field intensity enhancement since it has been designed to be as similar as possible to the reference antenna. To find better designs and the optimal magnitude of a in Eq. (8) will be a topic of future research.

Finally we want to mention that in this work we omit the refraction of fields at the antenna surface. This is a good approximation if the antenna material strongly deviates from an ideal metal (for a discussion see Sec. S6 of the Supplemental Material [29]).

Conclusion.—Reciprocity and Poynting's theorem can be combined to obtain a three-dimensional mode-matching framework for describing the optimal coupling between a quantum emitter and a plasmonic optical antenna. Based on this framework we identified two fundamental mode current

patterns for the optimal focusing of optical antennas. Making use of these new design rules for optical antennas the concept of the plasmonic cavity antenna has been developed, which outperforms a two-wire reference antenna.

The developed framework will help to unravel the full potential of focusing optical antennas and will help to optimize, e.g., tip enhanced Raman spectroscopy (TERS) tips and SERS substrates, making use of novel complex and surprising geometries [22,23]. Both the near-field and far-field coupling tasks of an optical antenna can be optimized rather independently yielding a large flexibility to optimize antenna performance for a variety of different tasks. Far-field detectors with a finite area can be implemented by a superposition of multiple dipoles. An extension to multiparticle multimode systems with retardation, where several double mode-matching conditions define the overall far field to near field conversion efficiency will help to better understand complex and large scale SERS-active substrates [24]. On the other hand, by deliberately avoiding far-field coupling and concentrating on the quantum emitter to antenna coupling only [4], nanocavities for strong light matter coupling can be devised.

T. F. acknowledges Katja Hoeflich for stimulating discussions. The work was funded by the Deutsche Forschungsgemeinschaft (DFG) (Grants No. HE5648/1-1 and No. CRC951).

*hecht@physik.uni-wuerzburg.de

[1] L. Novotny and N. van Hulst, Nat. Photonics **5**, 83 (2011).
[2] P. Biagioni, J.-S. Huang, and B. Hecht, Rep. Prog. Phys. **75**, 024402 (2012).
[3] A. Kinkhabwala, Z. Yu, S. Fan, Y. Avlasevich, K. Müllen, W. E. Moerner, and K. Muellen, Nat. Photonics **3**, 654 (2009).
[4] G. M. Akselrod, C. Argyropoulos, T. B. Hoang, C. Ciracì, C. Fang, J. Huang, D. R. Smith, and M. H. Mikkelsen, Nat. Photonics **8**, 835 (2014).
[5] P. Törmä and W. L. Barnes, Rep. Prog. Phys. **78**, 013901 (2015).
[6] T. B. Hoang, G. M. Akselrod, C. Argyropoulos, J. Huang, D. R. Smith, and M. H. Mikkelsen, Nat. Commun. **6**, 7788 (2015).
[7] M. E. Stewart, C. R. Anderton, L. B. Thompson, J. Maria, S. K. Gray, J. A. Rogers, and R. G. Nuzzo, Chem. Rev. **108**, 494 (2008).
[8] L. Novotny and S. J. Stranick, Annu. Rev. Phys. Chem. **57**, 303 (2006).
[9] S. A. Kalele, N. R. Tiwari, S. W. Gosavi, and S. K. Kulkarni, J. Nanophoton. **1**, 012501 (2007).
[10] P. Mühlschlegel, H.-J. Eisler, O. J. F. Martin, B. Hecht, D. W. Pohl, and P. Muhlschlegel, Science **308**, 1607 (2005).
[11] A. G. Curto, G. Volpe, T. H. Taminiau, M. P. Kreuzer, R. Quidant, and N. F. van Hulst, Science **329**, 930 (2010).
[12] J. Dorfmüller, R. Vogelgesang, W. Khunsin, C. Rockstuhl, C. Etrich, and K. Kern, Nano Lett. **10**, 3596 (2010).
[13] C. Sauvan, J. P. Hugonin, I. S. Maksymov, and P. Lalanne, Phys. Rev. Lett. **110**, 237401 (2013).
[14] P. T. s. Kristensen and S. Hughes, ACS Photonics **1**, 2 (2014).
[15] J.-J. Greffet, M. Laroche, and F. Marquier, Phys. Rev. Lett. **105**, 117701 (2010).
[16] A. E. Krasnok, A. P. Slobozhanyuk, C. R. Simovski, S. A. Tretyakov, A. N. Poddubny, A. E. Miroshnichenko, Y. S. Kivshar, and P. A. Belov, Sci. Rep. **5**, 12956 (2015).
[17] B. Hecht and L. Novotny, *Principles of Nano-Optics*, 2nd ed. (Cambridge University Press, Cambridge, England, 2012).
[18] J. Schwinger, L. L. J. Deraad, and K. A. Milton, *Classical Electrodynamics* (Westview Press, Boulder, Colorado, 1998), Chap. 12, p. 592.
[19] A. A. W. Snyder and J. D. Love, *Optical Waveguide Theory*, Science Paperbacks (Springer, New York, 1983), p. 734.
[20] P. Then, G. Razinskas, T. Feichtner, P. Haas, A. Wild, N. Bellini, R. Osellame, G. Cerullo, and B. Hecht, Phys. Rev. A **89**, 053801 (2014).
[21] T. Feichtner, O. Selig, and B. Hecht, Opt. Express **25**, 10828 (2017).
[22] A. García-Etxarri, P. Apell, M. Käll, and J. Aizpurua, Opt. Express **20**, 25201 (2012).
[23] R. Regmi, A. A. Al Balushi, H. Rigneault, R. Gordon, and J. Wenger, Sci. Rep. **5**, 15852 (2015).
[24] S. Schlücker, Angew. Chem., Int. Ed. Engl. **53**, 4756 (2014).
[25] K. H. Drexhage, in *Progress in Optics XII*, edited by E. Wolf (Elsevier, New York, 1974), pp. 163–232.
[26] Q. Bai, M. Perrin, C. Sauvan, J.-P. Hugonin, and P. Lalanne, Opt. Express **21**, 27371 (2013).
[27] P. T. Kristensen, R.-C. Ge, and S. Hughes, Phys. Rev. A **92**, 053810 (2015).
[28] E. A. Muljarov and W. Langbein, Phys. Rev. B **94**, 235438 (2016);
[29] See Supplemental Material at http://link.aps.org/supplemental/10.1103/PhysRevLett.119.217401 for several deeper aspects of the main paper: acquisition of quasi-normal-modes, analytical and numerical proof of the presented theory, discussion of field distortions in metal at optical frequencies and discussion of optical resonances in spherical metal shells.
[30] P. T. Leung and R. Chang, J. Opt. A: Pure Appl. Opt. **10**, 075201 (2008).
[31] J. Rahola, SIAM J. Sci. Comput. **21**, 1740 (2000).
[32] A. G. Polimeridis, M. T. H. Reid, S. G. Johnson, J. K. White, and A. W. Rodriguez, IEEE Trans. Antennas Propag. **63**, 611 (2015);
[33] O. D. Miller, A. G. Polimeridis, M. T. Homer Reid, C. W. Hsu, B. G. DeLacy, J. D. Joannopoulos, M. Soljačić, and S. G. Johnson, Opt. Express **24**, 3329 (2016).
[34] M. Kerker, D.-S. Wang, and H. Chew, Appl. Opt. **19**, 4159 (1980).
[35] R. Ruppin, J. Chem. Phys. **76**, 1681 (1982).
[36] G. Mie, Ann. Phys. (Berlin) **330**, 377 (1908).
[37] R. Carminati, J. J. Greffet, C. Henkel, and J. M. Vigoureux, Opt. Commun. **261**, 368 (2006).
[38] C. F. Bohren and D. R. Huffman, *Absorption and Scattering of Light by Small Particles* (Wiley, New York, 1983), p. 530.
[39] W. T. Doyle, Phys. Rev. B **39**, 9852 (1989).

[40] T. Feichtner, O. Selig, M. Kiunke, and B. Hecht, Phys. Rev. Lett. **109**, 127701 (2012).
[41] R. Olmon and M. Raschke, Nanotechnology **23**, 444001 (2012).
[42] C. Forestiere, M. Donelli, G. F. Walsh, E. Zeni, G. Miano, L. Dal Negro, and L. D. Negro, Opt. Lett. **35**, 133 (2010).
[43] P. Ginzburg, N. Berkovitch, A. Nevet, I. Shor, and M. Orenstein, Nano Lett. **11**, 2329 (2011).
[44] C. Forestiere, A. J. Pasquale, A. Capretti, G. Miano, A. Tamburrino, S. Y. Lee, B. M. Reinhard, and L. Dal Negro, Nano Lett. **12**, 2037 (2012).
[45] D. Macías, P.-M. Adam, V. Ruíz-Cortés, R. Rodríguez-Oliveros, and J. A. Sánchez-Gil, Opt. Express **20**, 13146 (2012).
[46] J. Enderlein, Appl. Phys. Lett. **80**, 315 (2002).
[47] L. Novotny, Phys. Rev. Lett. **98**, 266802 (2007).
[48] S. A. Kalele, S. W. Gosavi, J. J. Urban, and S. K. Kulkarni, Curr. Sci. **91**, 1038 (2006).
[49] The mode and the spectra were obtained numerically using Lumerical FDTD Solutions, using focused broadband ($\lambda = 550$–750 nm) Gaussian illumination (NA $= 1$, 3.9 fs pulse length). The gold material was implemented according to Ref. [50].
[50] P. G. Etchegoin, E. C. Le Ru, and M. Meyer, J. Chem. Phys. **125**, 164705 (2006).
[51] K. F. Lee, *Principles of Antenna Theory* (John Wiley & Sons Ltd, New York, 1984).
[52] S. Tretyakov, Plasmonics **9**, 935 (2014).